Turbine Blade Nonlinear Structural and Life Analysis

R. L. McKnight* and J. H. Laflen†
General Electric Company, Cincinnati, Ohio
and
G.R. Halford‡ and A. Kaufman§
NASA Lewis Research Center, Cleveland, Ohio

The utility of advanced structural analysis and life prediction techniques was evaluated for the life assessment of a commercial air-cooled turbine blade with a history of tip cracking. Three-dimensional nonlinear finite-element structural analyses were performed for the blade tip region. The computed strain-temperature history of the critical location was imposed on a uniaxial strain controlled test specimen to evaluate the validity of the structural analysis method. Experimental results indicated higher peak stresses and greater stress relaxation than the analytical predictions. Life predictions using the strainrange partitioning and frequency modified approaches predicted from 1200 to 4420 cycles and 2700 cycles to crack initiation, respectively, compared to an observed life of 3000 cycles.

Nomenclature

A, A', C_2	= coefficients in empirical equations
D_p	= plastic true strain at fracture in rapid tensile test
E	= modulus of elasticity
k, k', m, n	= exponents in empirical equations
N_f	= cycles to failure
N_{pc}	= cyclic life for $\Delta\epsilon_{pc}$
T	= temperature
t	= time
α	= mean coefficient of thermal expansion from room temperature to indicated temperature
β, β'	= exponents in empirical equations
$\Delta\epsilon$	= total strain range
$\Delta\epsilon_{pc}$	= inelastic strain range (tensile plasticity/compressive creep)
ϵ	= strain
ϵ_c	= creep strain
μ	= Poisson's ratio (elastic)
ν	= cyclic frequency
σ	= stress

Introduction

THE most critical structural requirements that aircraft gas turbine engines must meet result from the diversity of extreme environmental conditions in the turbine-section components. Accurate life assessment of the components under these conditions requires sound analytical tools and techniques, an understanding of the component operating environment, and comprehensive data on component materials. Inadequate understanding of any or all of these areas may result in either an overly conservative design which could impose a performance penalty on the engine or premature failure of the component.

Submitted June 11, 1982; presented as Paper 82-1056 at the AIAA/SAE/ASME 18th Joint Propulsion Conference, Cleveland, Ohio, June 21-23, 1982; revision received Oct. 12, 1982. This paper is declared a work of the U.S. Government and therefore is in the public domain.

*Manager, Nonlinear Analysis Methods, Aircraft Engine Business Group.
†Manager, Materials Life and Methods, Aircraft Engine Business Group.
‡Senior Researcher, Structures and Mechanical Technologies Division.
§Research Engineer, Structures and Mechanical Technologies Division.

Advanced nonlinear structural analysis techniques have become available in recent years to provide more reliable input to life predictions of life-limited turbine components. However, verification of these methods through application to well-documented failure case histories has been lacking.

The primary reason nonlinear stress analysis computer programs have not been used in hot section component design is because of the extensive computation time required for such applications. Furthermore, poorly defined material constitutive equations have hampered more general use of such computer programs.

In addition, several high-temperature low-cycle fatigue life prediction approaches have been proposed in recent years. These approaches have not yet been applied extensively to hot section components because critical evaluation through application to well-documented failure case histories has not been possible.

The objectives of this program were to evaluate the utility of these advanced structural analysis and life prediction techniques in the life assessment of hot section components. A particular goal was to assess the extent to which a cyclic three-dimensional finite-element analysis of a hot section component would improve the accuracy of the input information used in component life predictions. At the same time, new high-temperature life prediction theories such as strainrange partitioning (SRP)[1-3] and the frequency modified (FM)[4,5] approaches were to be applied and their adequacy judged.

A commercial air-cooled turbine blade with a well-documented history of cracking in the squealer tip region was selected as the vehicle for accomplishing the above objective. To perform the stress analysis for this turbine blade, a detailed three-dimensional model of the blade tip region was constructed which consisted of eight-noded isoparametric finite elements (580 elements and 1119 nodes).

To perform the cyclic nonlinear analysis, a commercially available program, ANSYS, was chosen. For this analysis, previously determined temperature-dependent cyclic stress-strain curves and creep data were used. The kinematic hardening option was selected for the plasticity analysis, and the creep analysis was performed with the time-hardening rule. Seven complete stress-strain cycles were computed, at which time shakedown was determined to have occurred. The computed strain-temperature history at the critical location was used to program a thermomechanical test of an axially loaded specimen. The results of these analyses and the thermomechanical tests were used to make life predictions. Comparisons are made between predictions of life and the life observed in blades run in an engine test at General Electric.

Problem Description

A stage 1 high-pressure turbine blade of a commercial aircraft engine was selected as the hot section component to be analyzed because of its significant creep-fatigue problems.[6] These blades are hollow, air-cooled, and paired together on a single three-tang dovetail. Figure 1 shows one such blade and indicates the region of analysis. The airfoil has a span of 4.57 cm, a chord width of 3.30 cm, and a hub to tip radius ratio of 1.13. The material is cast Rene' 80 with an aluminide, CODEP-B, coating; temperature-dependent physical properties for this alloy are presented in Table 1. The cyclic stress-strain and monotonic creep properties used in the analysis are given in Tables 2 and 3, respectively.

The failure mode for this component is well defined. The blade has a tip cap just below the actual tip of the blade, this configuration being designated a "squealer tip." Radial cracks occur in the squealer tip region. These cracks are a problem on all such blades; thus the problem being addressed is one common to many engine manufacturers.

Figure 2 shows the mission cycle used for analysis in terms of turbine inlet and compressor discharge temperatures and engine speed. This cycle is typical of field engine experience with the exception of the condensed cruise time. Transient thermal stresses are induced primarily through the engine acceleration and thrust reversal transients. Creep occurs mainly during the interval from 6.7 (end of acceleration) to 200 s (beginning of thrust reversal).

Transient and steady-state three-dimensional heat transfer analyses were conducted utilizing film coefficients and boundary conditions obtained from blade tip model test data. Calculated temperatures were found to be in good agreement with thermocouple measurements from factory test engines. Metal temperatures for the leading and trailing edges, the bulk temperature at the blade tip, and the temperature of a point in the cap as a function of elapsed time during the cycle are shown in Fig. 3. The calculated metal temperature at the critical location (crack initiation site) is shown in Fig. 4. This location is at the blade tip on the suction side toward the trailing edge.

Factory engine testing was conducted for the blade geometry studied. Unlike a typical flight cycle, the factory testing included two additional idle-to-takeoff loadings per major cycle. These more rapidly applied extra cycles were imposed to decrease factory engine test time and hence cut costs. Their influence was accounted for in all life prediction calculations.

The particular combination of factory cycles and blade geometry studied here involved 16 blades and 1000 factory cycles (3000 stress-strain loading cycles). At the end of the 3000 stress-strain cycles, the blades were removed and the extent of cracking was documented. Of the 16 blades, one had cracked just to the tip cap, ten had cracked below the tip cap,

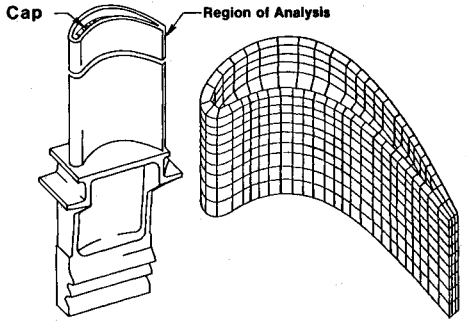

Fig. 1 Stage 1 high-pressure turbine blade and finite-element model.

Table 1 Rene' 80 temperature-dependent material properties

Temperature, °C	E, MPa	μ	α, %/°C
21	$207.7\times10^{+3}$	0.310	12.4×10^{-4}
93	204.2	0.313	12.4
204	198.7	0.315	12.4
316	193.2	0.318	12.6
427	187.7	0.320	13.0
538	181.5	0.325	13.3
649	174.6	0.328	13.7
760	166.3	0.330	14.4
871	156.6	0.340	15.1
982	142.8	0.350	16.2
1093	116.6	0.363	17.5
1149	93.8	0.370	18.4

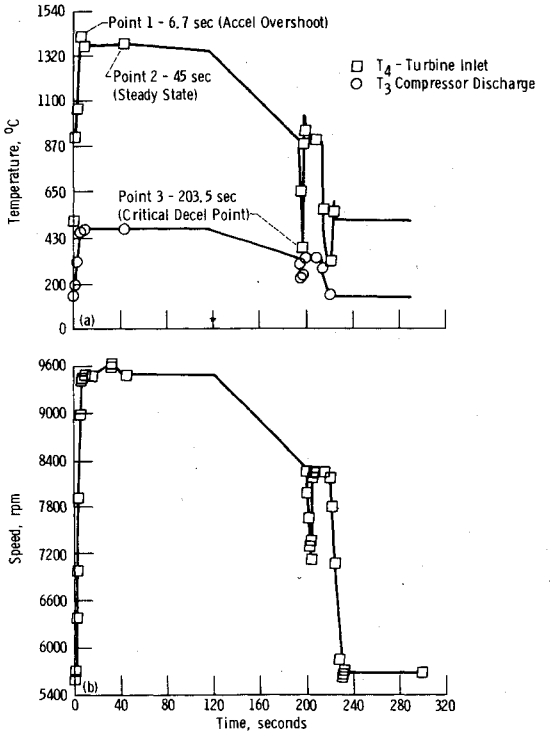

Fig. 2 Mission cycle used for analysis.

Table 2 Rene' 80 cyclic stress-strain data

	Stress, MPa							
Strain, %	21°C	649°C	871°C	927°C	982°C	1038°C	1093°C	1149°C
0.05	103.8	87.3	78.3	74.9	71.4	64.9	58.3	46.9
0.1	207.7	174.6	156.6	142.8	124.2	113.9	103.5	88.3
0.2	415.4	349.2	300.2	269.1	227.7	181.5	155.3	129.7
0.4	797.0	662.4	527.9	455.4	383.0	248.4	207.0	265.6
0.6	1014.3	879.8	714.2	621.0	476.1	274.6	227.7	181.5
0.8	1200.6	1040.5	843.9	734.9	523.0	285.0	227.7	186.3
1.0	1361.4	1164.7	931.5	807.3	543.7	289.8	227.7	186.3
1.2	1480.1	1262.7	1014.3	879.8	558.9	289.8	238.1	186.1
1.5	1552.5	1304.1	1055.7	921.2	558.9	300.2	238.1	186.3

and five had cracked below the tip cap, and had changed direction. Since the tip cap was 3.8 mm below the blade tip, this length and 3000 stress-strain cycles were used as the criteria for judging the results of the life predictions.

Analytical Procedure

The ANSYS Program[7] was chosen for use in the three-dimensional cyclic inelastic structural analysis of the turbine blade tip region because of its extensive capabilities and its ability to solve large structural problems. The ANSYS Program uses an initial strain approach for determining plasticity effects. This method computes a reference elastic material stiffness and corresponding elastic strains for each time step. The procedure uses an iterative solution technique with a constant triangularized stiffness matrix and a load vector that is modified after each iteration so that the stress

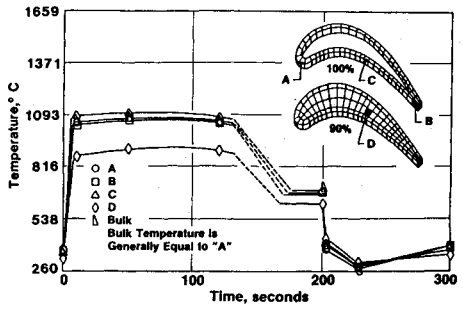

Fig. 3 Blade temperature—time profile.

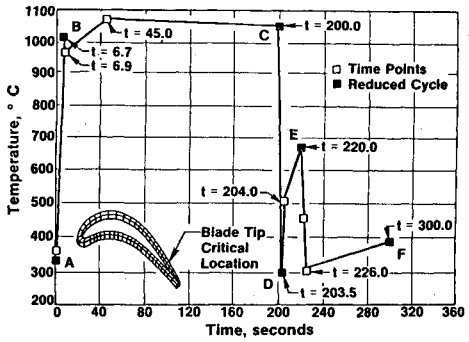

Fig. 4 Blade metal temperature vs time at critical location.

Table 3 Rene' 80 creep properties

Temperature, °C	A, MPa	m	n
649	4347	2.54	0.452
871	398	5.19	0.685
927	315	4.60	0.813
982	249	3.65	0.890
1038	222	2.65	0.920
1093	197	2.00	0.923
1149	176	1.43	0.924

calculated in the next iteration approaches the stress that the material can support at the strain. Each time step consists of a sufficient number of iterations, based on a single set of boundary conditions, so that convergence criteria are met. Plasticity convergence criteria are met whenever the ratio of the plastic strain increment to the elastic strain for all elements is less than 1% (recommended). Reversed loading with plasticity was modeled using the ANSYS kinematic hardening option. This option assumes that yielding in the reverse direction occurs when the stress excursion equals twice the virgin yield stress.

For creep analyses, the creep rates are determined from the stresses computed after the plasticity solution has been calculated. The creep law equation is of the form

$$\epsilon_c = (\sigma/A)^m (t)^n \tag{1}$$

Creep calculations are handled by an incremental technique similar to that used for plasticity. The iterative procedure is completed when the ratio of the creep strain increment to the elastic strain for all elements is less than a recommended value of 0.25.

Initially, the mission cycle was subdivided into several load-time steps for the inelastic analysis. Inspection of the results from the first inelastic analysis cycle suggested that the number of steps could be reduced to six provided that a sufficient number of iterations were permitted so that the convergence criteria could be satisfied. The initial cycle was rerun using the reduced number of increments and excellent agreement was found with the original inelastic analysis results. Time steps for both the original and reduced (points A-F) cycles are illustrated in Fig. 4.

In all subsequent cycles, plasticity analyses were performed using the reduced number of increments. Creep analyses were conducted for the relatively stable steady-state temperature increment from B to C in Fig. 4. The cyclic inelastic analysis was continued for seven cycles because of lack of initial stabilization of the stress-strain hysteresis loop at the critical crack initiation location. Each reduced cycle with six time steps required approximately 183 min of execution time on a CDC 176 computer.

Finite-Element Model

A three-dimensional finite-element model (Fig. 1) of the component blade tip above the 75% span was constructed of 580 eight-noded isoparametric brick elements with 1119 nodes. A detailed, exploded view of this model depicting the squealer tip, tip cap, and spar as discrete three-dimensional components is shown in Fig. 5. The spanwise length of the model was sufficient to preclude interference between the applied bottom boundary conditions and the squealer tip region, which is the region of interest.

The isoparametric element was chosen because of its capability to model almost any three-dimensional geometry and temperature distribution very accurately. The eight-noded brick was used exclusively because the 16- and 20-noded bricks in the ANSYS element library lacked creep capabilities. Specifically, the eight-noded brick element is an isoparametric hexahedral box element with eight nodal points and 33 degrees of freedom (three displacement components at

Table 4 Results of turbine blade tip structural analyses (all results are for principal direction normal to radial crack at critical location)

		Inelastic		
	Elastic	Cycle 1	Cycle 2	Cycle 7
Maximum total strain, %	0.025	−0.05	−0.062	−0.0829
Minimum total strain, %	−0.2925	−0.3582	−0.371	−0.3918
Total strain range, %	0.3175	0.3082	0.3090	0.3089
Mean stress, MPa	−164.9	−12.9	33.7	80.5

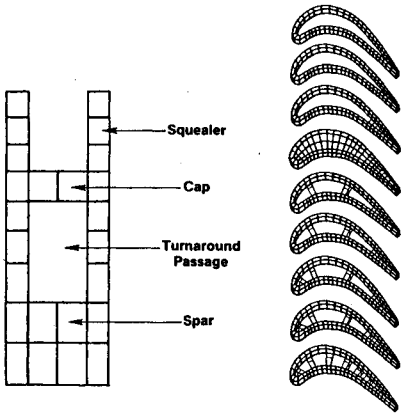

Fig. 5 Finite element model of blade tip.

each of the eight nodal points and 9 internal degrees of freedom). The displacement field at any point within the element is assumed to be quadratic, giving rise to strain components which vary linearly across the element. For this reason, structures in which bending effects are significant can be modeled using relatively few elements. Thus it was possible to model the blade tip region using only one element in the thickness direction.

Boundary conditions were applied to constrain all nodes at the base of the model to lie on the 75% span plane of the airfoil. Additional boundary conditions were applied to prevent rigid body motion in this plane.

Discussion of Results

The critical location for crack initiation is at the blade tip on the suction surface toward the trailing edge. Results of both elastic and inelastic structural analyses indicated that the region of the finite-element model with the largest total strain range was coincident with the observed crack initiation site. In the following discussion, the computed principal stresses and strains normal to the radial crack direction at the critical location were used to define the stress-strain response.

Figure 6 shows the stress-strain response at the critical location computed from the ANSYS *elastic* analysis. Letter designations given on the hysteresis loop in Fig. 6 are consistent with those given for the temperature response in Fig. 4. During the heating portion of the cycle from startup (A) to acceleration overshoot (B), the critical location underwent compressive straining. The minimum strain occurred after 200 s of heating (C). Thrust reversal caused the strain to reverse direction with the maximum strain occurring at (D).

Predicted results from the blade tip *inelastic* analysis for the first, second, and seventh mission cycles are shown in Fig. 7 and Table 4. Again the letter designations are for reference to the temperature response in Fig. 4, and the prime superscripts apply to the second cycle. The stress-strain hysteresis loops in Fig. 7 were constructed by connecting, with straight lines, the computed results for the six time steps in the reduced cycle.

Plasticity analyses were performed during the heating portion of the cycle from A to B and creep analyses during the relatively steady-state portion from B to C. The remainder of the cycle from C to F involved nominally elastic response. Although calculations did not reveal the presence of inelastic straining during the cooling portion of the cycle, some small amount of plastic strain is to be expected. The discrepancy between calculation and expectation results from the following argument. The calculations are based on a linear segmented stress-strain representation that is too coarse to represent accurately the gradual early deviation from linear elasticity that is associated with the classical Bauschinger effect in cyclic loading. Any tensile inelastic deformation would be expected to be plastic (time-independent) and of a comparable magnitude to the inelastic creep strain encountered in compression. For all practical purposes, the cycle approaches a pure $\Delta\epsilon_{pc}$ condition.

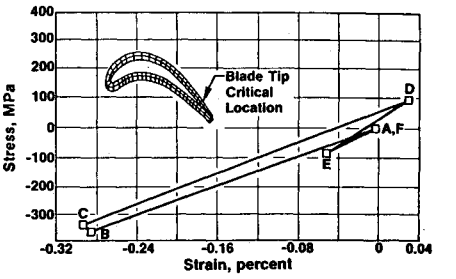

Fig. 6 Elastic analysis results—stress-strain response at critical location.

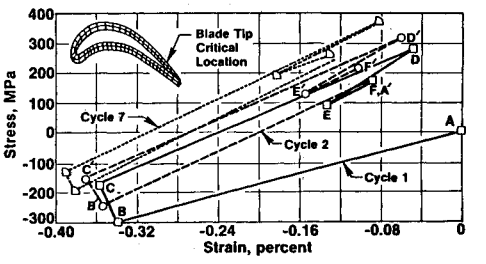

Fig. 7 Inelastic analysis results—stress-strain response at critical location.

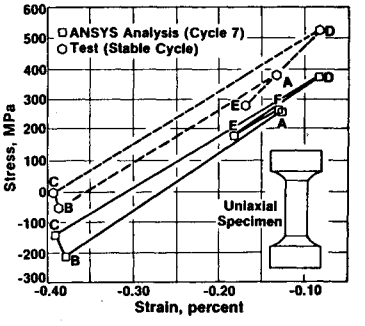

Fig. 8 Comparison of uniaxial thermomechanical test and inelastic analysis results.

As shown in Fig. 7, continued cycling produced hysteresis loops that moved progressively in the negative strain direction, with larger peak tensile stresses during the cooling portion of the cycle. Additionally, the predicted creep strain increment per cycle decreased with each increasing cycle as the stress level at the hot end of the cycle stabilized. While complete hysteresis loop stabilization had not occurred by the seventh cycle, the maximum change in total strain between the sixth and seventh cycles for any comparable points was less than 0.0035% strain. The corresponding maximum stress change was less than 6.9 MPa. This was felt to be adequate stabilization for analysis requirements, and additional computing costs due to further inelastic cyclic analysis was not warranted. The inelastic strain range for the seventh cycle was approximately 0.013%. A comparison, in Table 4, of the computed total strain ranges from the ANSYS elastic and inelastic analyses reveals a very small difference of less than 3%.

To evaluate the validity of the blade inelastic analysis, a thermomechanical fatigue (TMF) test was conducted using a smooth uniaxial test specimen. The experimental system[6] is capable of following a prescribed strain-temperature time history. The predicted total strain and temperature histories for the seventh cycle of the ANSYS inelastic analysis were used to define the specimen test conditions. The TMF testing demonstrated that the cyclic stress-strain response stabilized by the sixth cycle, and no significant stress relaxation occurred on subsequent cycling. The measured inelastic strain range was 0.03% and was of the $\Delta\epsilon_{pc}$ type.

In conjunction with the TMF test program, an ANSYS inelastic analysis was conducted using a simple two-dimensional finite-element model to represent the specimen test section. This analysis used the same material models as the blade inelastic analysis and followed the same strain-temperature history as the test specimen. The simplicity of this analysis, as compared to the blade structural analysis, permitted a larger number of cycles to be run economically.

A comparison of the TMF analytical and test results is presented in Fig. 8. The analytical results are for the seventh cycle, by which time further stress ratcheting was minor and the response could be considered to be essentially stabilized.

The test cycle exhibits a higher peak stress at cooldown (D) and a lower compressive stress than was predicted from the inelastic analysis. On the initial cycle, the observed stress relaxation was approximately three times greater than that of the analysis. This indicates the high-temperature creep model/properties that were used require modification. It should be noted that only a small amount of short-time creep data exist at these stress-temperature levels owing to the difficulty in performing such tests. Also, static creep test results were used to represent cyclic creep behavior. Correct determination of the thermomechanical plasticity and creep response is critical for the life prediction of the component.

Life Prediction

Calculations of the expected cyclic crack initiation lifetime of the blade tip were made using two advanced high-temperature low-cycle fatigue life prediction theories: strainrange partitioning (SRP) and the frequency modified (FM) approaches. In the current paper, we present only the pertinent equations and their respective constants, and refer the reader to Ref. 6 for greater details on additional properties of the cast Rene' 80 blade material. Any influence that the CODEP-B aluminide coating may have had on the material behavior has not been accounted for specifically in the life calculations.

Life Predictions by SRP

Reference 8 provides the equations for the four SRP life relations for Rene' 80 measured at 1000°C. Only the $\Delta\epsilon_{pc}$ inelastic strain range component is present in the current problem; thus only the N_{pc} life relation is needed:

$$\Delta\epsilon_{pc} = 11.6 (N_{pc})^{-0.64} \tag{2}$$

at 1000°C, where $\Delta\epsilon_{pc}$ is in percent. Since the tensile half of the cycle involves plastic strain that is encountered near the lowest end of the temperature cycle (i.e., 344°C), Eq. (2) should be adjusted to reflect the tensile plastic straining capacity at 344°C rather than at 1000°C. Procedures for making this adjustment are based upon the ductility normalized-SRP life relations.[9] The adjustment is made to the coefficient in Eq. (2). The ratio (0.244) of the tensile plastic ductility, D_p, measured at 344°C ($D_p = 9.9\%$) to that at 1000°C ($D_p = 40.6\%$) is multiplied times the 11.6 coefficient to scale Eq. (2) from applicability at 1000°C to applicability at 344°C where the straining capacity is less by the 0.244 factor. Hence

$$\Delta\epsilon_{pc} = 2.8 (N_{pc})^{-0.64} \tag{3}$$

at 344°C.

For values of $\Delta\epsilon_{pc} = 0.03$ (from the thermomechanical test) and 0.013% (from inelastic ANSYS analysis), predicted cyclic crack initiation lives are 1200 and 4420, respectively. These bracket the observed life of 3000 cycles for the turbine blade tip.

Life Prediction by the FM Approach

The FM equation is given by

$$\Delta\epsilon = (A'/E)(N_f)^{-\beta'}(\nu)^{k'l} + C_2 (N_f)^{-\beta}(\nu)^{\beta(l-k)} \tag{4}$$

The cyclic frequency is 0.0049 Hz for the current problem. Values of the constants have been well documented[6] for Rene' 80 at 980°C. Supplementary results[6] at temperatures up to 1100°C indicate an insensitivity of the fatigue characteristics to temperatures within this narrow regime (980-1100°C). Assuming the FM equation can be applied to a variable temperature problem by evaluation of the constants at the maximum temperature of the cycle, Eq. (4) becomes

$$\Delta\epsilon = 0.489 (N_f)^{-0.112} + 13.8 (N_f)^{-0.614} \tag{5}$$

For the blade tip total strain range of 0.31% (Table 4), a predicted crack initiation life of 2700 cycles is determined from Eq. (5) by iteration. By comparison, the observed life of the blade tip was 3000 cycles. Although the cyclic lifetime is accurately calculated by the FM approach in this case, the results may be fortuitous because Eq. (5) implies that the elastic and inelastic strain ranges (the first and second right-hand terms, respectively) are 0.20 and 0.11%, respectively. This is in sharp contrast to the experimental TMF values of 0.28 and 0.03% for the two respective strain range components. Obviously, the applicability of Eq. (4) to variable temperature cycling conditions requires guidance above and beyond that found in the literature.

Summary of Results

The results of the turbine blade nonlinear structural and life analyses can be summarized as follows:

1) The total strain range at the critical cracking site was calculated using both elastic and inelastic ANSYS analyses. The total strain range values were within less than 3% of each other, thus indicating the potential value of the simpler, much less expensive, elastic analysis.

2) Tests of a uniaxial strain controlled specimen following the same strain-temperature history as computed at the blade tip crack initiation location showed that the stress-strain response stabilized by the fourth cycle. Analytical simulation of this experiment demonstrated later stabilization of the stress-strain response, higher peak stresses, and a smaller amount of stress relaxation than the test results indicated. These discrepancies between analysis and experiment suggest that the creep model and/or data did not accurately represent the material cyclic time-dependent behavior.

3) The three-dimensional structural analyses produced results in qualitative agreement with the limited experimental evidence. The maximum strain ranges were predicted for the blade tip region where actual cracking occurred.

4) Cyclic crack initiation life of the blade tip was calculated by the strainrange partitioning (SRP) and frequency modified (FM) approaches and compared to the observed life of 3000 cycles from factory engine testing. Predicted lives ranged from 1200 to 4420 cycles for SRP depending upon the magnitude of the expected inelastic strain range. Based upon a calculated total strain range of 0.31%, the FM method predicted a crack initiation life of 2700 cycles.

References

[1] Manson, S.S., Halford, G.R., and Hirschberg, M.H., "Creep-Fatigue Analysis by Strain-Range Partitioning," *Symposium on Design for Elevated Temperature Environment*, American Society of Mechanical Engineers, New York, N.Y., 1971, pp. 12-28.

[2] Hirschberg, M.H. and Halford, G.R., "Use of Strainrange Partitioning to Predict High-Temperature Low-Cycle Fatigue Life," NASA TN D-8072, 1976.

[3] *Characterization of Low Cycle High Temperature Fatigue by the Strainrange Partitioning Method*, AGARD-CP-243, Technical Editing and Reproduction Ltd., London, 1978.

[4] Coffin, L.F. Jr., "Fatigue At High Temperature," *Fatigue At Elevated Temperatures*, ASTM STP 520, American Society for Testing and Materials, Philadelphia, Pa., 1973, pp. 5-34.

[5]Coffin, L.F., "A Review of Fatigue Predictive Methods in the Regime where Inelastic Strains Dominate," *Methods for Predicting Material Life in Fatigue*, American Society of Mechanical Engineers, New York, N.Y., 1980, pp. 1-24.

[6]McKnight, R.L., Laflen, J.H., and Spamer, G.T., "Turbine Blade Tip Durability Analysis," NASA CR-165268, 1981.

[7]Kohnke, P.C., "ANSYS Engineering Analysis System Theoretical Manual," Swanson Analysis Systems, Inc., Elizabeth, Penn., 1977.

[8]Halford, G.R. and Nachtigall, A.J., "Strainrange Partitioning Behavior of the Nickel-Base Superalloys, Rene' 80 and IN 100," AGARD CP 243, 1978, pp. 2-1-2-14.

[9]Halford, G.R., Saltsman, J.F., and Hirschberg, M.H., "Ductility Normalized-Strainrange Partitioning Life Relations for Creep-Fatigue Life Prediction," *Proceedings of the Conference on Environmental Degradation of Engineering Materials*, Virginia Technical Printing Department, Virginia Polytechnic Institute and State University, Blacksburg, Va., 1977, pp. 599-612.